DOI: 10.1002/chem.200801208

Bistable Molecular Switches Based on Linkage Isomerization in Ruthenium Polypyridyl Complexes with a Ligand-Bound Ambidentate Motif

Olof Johansson,* Linus O. Johannissen, and Reiner Lomoth*[a]

Abstract: Electron-transfer-induced linkage isomerization was investigated in a series of bis-tridentate Ru polypyridyl complexes $[Ru(L\text{-}X\text{-}OH)(Y\text{-}tpy)]^{2+}$ with ambidentate ligand L-X-OH = bpy-C(R)(OH)-py (bpy = 2,2′-bipyridine; py = pyridine; R = H, Me, Ph, or *t*Bu) and spectator ligand Y-tpy (tpy = 2,2′:6′,2″-terpyridine; Y = *p*-tolyl, *p*-$PhCO_2Me$, Cl, OEt, *N*-pyrrolidine). The ligand-bound ambidentate motif switches reversibly between N and O coordination in the Ru^{II} and Ru^{III} state, respectively. The potentials of the $Ru^{III/II}$ couple differ by about 0.5 V between the isomers, and this results in a bistable electrochemical response of the molecular switches. The effects of structural modifications in form of substituents on the linking carbon atom of the ambidentate ligand and on the central pyridine moiety of the spectator ligand were investigated by electrochemical and computational methods. Differences in isomerization behavior span six orders of magnitude in rate constants and two orders of magnitude in equilibrium constants. The results can be interpreted in terms of steric and electronic substituent effects and their influence on rotational barriers, ligation geometry, and electron deficiency of the metal center.

Keywords: ambidentate ligands · electrochemistry · isomerization · ruthenium · tridentate ligands

Introduction

The design and synthesis of molecular switches for potential use in molecular electronic devices has been an active area of research in recent years.[1–5] While single-molecule-based devices are still a distant goal, approaches based on the combination of molecular materials with nanomaterials very recently resulted in functional devices. Probably the most prominent example is a 160 kbit molecular RAM with 10^{11} bits cm^{-2}, a density that is projected for 2020 with today's DRAM technology. The hybrid device is based on a monolayer of bistable molecular switches in the form of rotaxanes that are electrochemically addressed via a cross-bar architecture of nanowires (Si, Ti).[6] Such applications of molecular switches in memory devices require that the switching process is characterized by a hysteretic response, that is, the system can exist in either one of two states for a range of values of an external parameter.[7,8] A general approach to molecular switches that show hysteresis-like behavior relies on redox-induced structural changes. Based on, for example, electrostatic or inductive effects, suitable structural alterations can result in a major displacement of the electrochemical potentials required to trigger and to reverse the process. At any potential in between, the system can exist in either oxidation state, depending on the electrochemical history (Scheme 1).

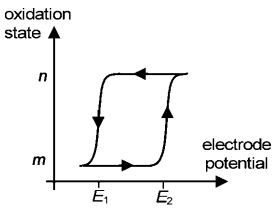

Scheme 1.

Molecular assemblies that display such bistability[9] include copper complexes of tetradentate ditopic pyridyl ligands for reversible assembly/disassembly of helicate structures,[10–13] supramolecular assemblies such as rotaxanes and catenanes based on aromatic acceptor–donor interactions or transition metal (copper) complexes,[14–20] oligophenylene derivatives for reversible C–C bond-breaking/bond-forming reactions,[21–26] and metal complexes containing ambidentate ligands that undergo redox-induced linkage isomerization.[27–34] Transition metal complexes of ambidentate ligands are particularly interesting, since sizeable potential separations can be invoked by small-amplitude molecular motions. This should render these systems particularly suitable for

[a] Dr. O. Johansson, Dr. L. O. Johannissen, Dr. R. Lomoth
Department of Photochemistry and Molecular Science
Uppsala University, Box 523, 75120 Uppsala (Sweden)
Fax: (+46) 18-471-6844
E-mail: olof.johansson@fotomol.uu.se
reiner.lomoth@fotomol.uu.se

Supporting information for this article is available on the WWW under http://dx.doi.org/10.1002/chem.200801208.

surface confinement and possible use in solid-state devices. Furthermore, the complexes are potentially more synthetically accessible than, for example, supramolecular assemblies, and the switching behavior and electrochromic properties of the metal complex can be tuned by modification of the spectator ligands. As a paradigm of this concept ruthenium-based complexes with ambidentate sulfoxide ligands have been extensively studied and shown to undergo S→O isomerization on metal oxidation and revert to S coordination on re-reduction.[27–33] However, most of these studies have used monodentate sulfoxide ligands, for which substitution reactions of the switching ligand are a potential problem.[30] In addition, the switching kinetics are frequently slow in at least one direction, and this would impede rapid writing and erasing of a molecular memory.

We previously investigated bis-tridentate ruthenium polypyridyl complexes that exhibit molecular hysteresis in the form of a bistable electrochemical response (Scheme 2) that arises from electron-transfer-induced linkage isomerization of an ambidentate ligand.[35,36] In contrast to previous examples of electrochemical bistability based on linkage isomerism, the ambidentate unit of these molecular switches is ligand-bound and thus does not dissociate from the complex in the course of isomerization. Reversible isomerization between the all-pyridine coordinated form (N_6) and the O-coordinated form (N_5O) is triggered by metal-centered oxidation or reduction. The better donor ability of the O ligand renders the potential of the $Ru^{III/II}N_5O$ couple about 0.5 V less anodic and thus results in the desired electrochemical bistability (Scheme 2).

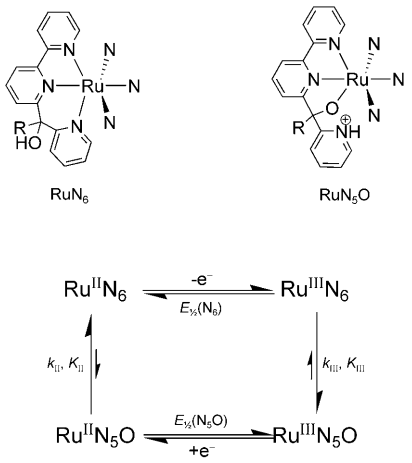

Scheme 2.

For complex **1** with the ambidentate ligand L-Me-OH we could demonstrate that interconversion between the two states is rapid in both directions with isomerizations on the millisecond timescale.[35] With their synthetic versatility this type of ruthenium complexes are hence interesting candidates for molecular memories. The pronounced absorption changes associated with bleaching of the metal-to-ligand charge-transfer (MLCT) band on oxidation to the Ru^{III} state provide an additional means of reading the state of the memory and could have potential applications for electrochromic materials with a hysteretic response.[37]

Here we report on a series of complexes that differ in the composition of either the ambidentate ligand (**1**–**4**) or the orthogonal 2,2′:6′,2″-terpyridyl (tpy) ligand (**5**–**8**).

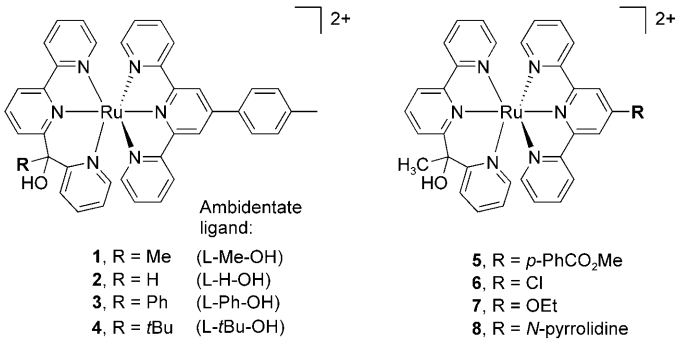

The isomerization reactions of these complexes were investigated by electrochemical and computational methods. Within the series, differences in square scheme parameters that characterize the ECEC mechanism can be interpreted in terms of steric hindrance and strain in the ambidentate unit as well as electronic substituent effects communicated via the spectator ligand. These results are directly relevant to the rational design of molecular switches based on this motif, including strategies for immobilization and incorporation into larger molecular assemblies.

Results and Discussion

Synthesis and characterization: The new ambidentate polypyridyl ligands L-H-OH and L-*t*Bu-OH were synthesized in analogy to the previously reported L-Me-OH[38] and L-Ph-OH[36] by reaction of 6-lithio-2,2′-bipyridine with 2-pyridinecarboxaldehyde and 2,2-dimethyl-1-(2-pyridyl)propanone, respectively, in THF/diethyl ether at −78 °C. Heteroleptic ruthenium(II) complexes **3**–**8** were subsequently prepared as originally reported for complex **1**[38] by first heating equimolar quantities of $[RuCl_2(dmso)_4]$ and Y-tpy in refluxing chloroform to form the $[RuCl_2(dmso)(Y\text{-}tpy)]$ intermediates according to the procedure developed by Ziessel and coworkers.[39] Without further purification, these compounds were then treated with ligands L-X-OH in refluxing ethanol/water to form heteroleptic complexes $[Ru(L\text{-}X\text{-}OH)(Y\text{-}tpy)]^{2+}$, which were isolated as PF_6^- salts after chromatographic purification on silica.

The synthesis of complex **2** proved to be more problematic due to facile oxidation of L-H-OH by air to give the corresponding ketone when coordinated to Ru^{II} (Scheme 3).

Both **2** and oxidation product **2a** formed during the reaction, whereby the latter could be readily identified by NMR

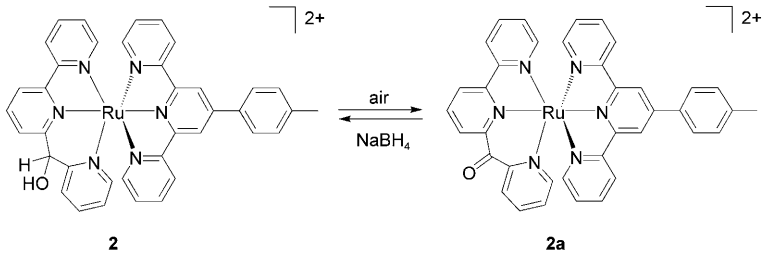

Scheme 3.

spectroscopy and mass spectrometry.[38] By using microwave heating and shorter reaction times, **2** could be isolated as the main product. On storage, **2** was slowly oxidized to **2a**, but the mixture was readily converted to **2** by treatment with $NaBH_4$.

The ^{1}H NMR spectra of **1**–**8**, recorded in CD_3CN, are complicated due to the low symmetry (point group C_1) of the complexes. As previously established from the ^{1}H NMR spectrum and solid-state structure,[35,38] the L-Me-OH ligand in **1** binds to Ru^{II} in an N,N,N mode. The same bonding mode holds for all L-X-OH ligands in **2**–**8**, as evidenced by the similarities in the UV/Vis absorption spectra and electrochemical behavior. The absorption spectra in the visible region are dominated by intense MLCT absorption bands at λ_{max} = 472–487 nm (Table 3), typical for all-pyridine-coordinated ruthenium(II) polypyridyl complexes. The complexes were further characterized by ESI mass spectrometry and elemental analyses, which were in accordance with the assigned structures. Complex **7**, however, differed from the calculated elemental composition regardless of repeated precipitation with NH_4PF_6 and recrystallization, probably due to minor salt impurities.

Electrochemistry: The electron-transfer-induced isomerization reactions were investigated by cyclic voltammetry (0.01–10000 $V s^{-1}$) and controlled-potential electrolysis to infer the kinetic and thermodynamic parameters of the ECEC mechanism. The electronic absorption spectra of the isomerization products were obtained by UV/Vis spectroelectrochemistry.

Parent complex: The voltammetric behavior of parent complex **1** (Figure 1) is characteristic for all complexes that exhibit rapid and essentially complete isomerization. The voltammograms at low scan rates are characterized by an irreversible anodic wave (1) and an irreversible cathodic wave (2) separated by about 0.5 V. At intermediate scan rates the counter-peak of the anodic wave emerges at the expense of the cathodic peak, and two quasireversible waves are observed on equilibration during subsequent scans. At the highest scan rates only one quasireversible wave is observed, which is either (1) or (2) depending on the initial scan direction.

As previously reported, this behavior of **1** can be rationalized in terms of an ECEC mechanism with two electron-transfer-induced isomerization reactions (Scheme 2). The corresponding square-scheme parameters are listed in Table 1.[40] They were determined from digital simulations (Figure 1) that consistently reproduce the experimental data over the entire range of scan rates. Oxidation of $Ru^{II}N_6$ to $Ru^{III}N_6$ gives rise to the anodic peak at about 0.8 V and triggers fast isomerization to the $Ru^{III}N_5O$ isomer. Reduction of the N_5O isomer occurs at much less positive potential, and the transiently generated $Ru^{II}N_5O$ complex transforms rapidly into the more stable $Ru^{II}N_6$ isomer. Oxidation of the $Ru^{II}N_5O$ isomer can, however, be observed at intermediate scan rates (Figure 1c) or more clearly in voltammograms starting from $Ru^{III}N_5O$ with scan rates that can compete with k_{II} (Fig-

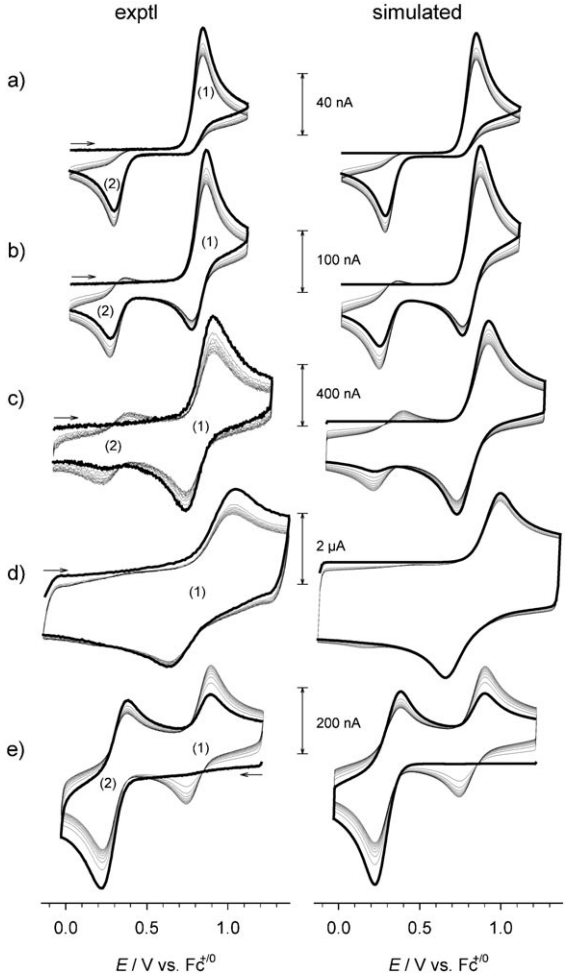

Figure 1. Cyclic voltammograms of **1** (6 mM) in acetonitrile with 0.6 M $TBAPF_6$ (left) and digital simulations with the parameters from Table 1 (right). Scan 1 (thick line) and scans 2–10 (thin lines) at a Pt microdisk electrode (∅ 25 µm). Scan rates: 10 (a), 100 (b), 1000 (c), 10000 (d), and 500 $V s^{-1}$ (e).

Table 1. Thermodynamic and kinetic characteristics of electrochemically induced isomerizations in acetonitrile solution[a] at 298 K.

Compd[b]	$E_{1/2}(N_6)$ [V][c]	$E_{1/2}(N_5O)$ [V][c]	k_{III} [s^{-1}]	K_{III}	k_{II} [s^{-1}]	K_{II}
1	0.82	0.31	2.5×10^{2}	2×10^{2}	8×10^{2}	2.1×10^{6}
2	0.83	_[d]	_[d]	_[d]	_[d]	_[d]
3[e]	0.82	0.28	4	5×10^{1}	7×10^{1}	2.7×10^{7}
4	0.81	0.25	5.3×10^{-4}	2.7	≈0.1	1.1×10^{9}
5	0.81	0.30	2.7×10^{2}	2×10^{2}	6×10^{2}	2.1×10^{6}
6	0.86	0.33	6.5×10^{2}	4×10^{2}	4×10^{2}	2.3×10^{6}
7	0.74	0.27	3×10^{2}	1×10^{2}	3×10^{2}	9×10^{5}
8	0.60	0.15	15	12	5×10^{2}	3.4×10^{6}

[a] With 0.6 M $(n\text{-}C_4H_9)_4NPF_6$ as supporting electrolyte. [b] As PF_6^- salts. [c] Versus ferrocenium/ferrocene, ±0.02 V. [d] No isomerization. The $Ru^{III/II}$ couple of the oxidation product has a half-wave potential of $E_{1/2}=$ 0.96 V, in agreement with that of isolated keto analogue **2a**.[38] [e] Data from ref. [36].

Table 2. Activation parameters for the isomerization reactions of **1**.

Reaction	E_a [kJ mol^{-1}]	$\ln A_s$	$\Delta H^{\neq}$[c] [kJ mol^{-1}]	$\Delta S^{\neq}$[d] [J mol^{-1} K^{-1}]
$Ru^{II}N_5O\rightarrow Ru^{II}N_6$[a]	38.1	22.3	35.8	−67
$Ru^{III}N_6\rightarrow Ru^{III}N_5O$[a]	49.6	25.8	47.3	−39
$Ru^{II}N_6\rightarrow(Ru^{II}N_5O)$-H[b]	79.4[e]	25.1[e]	76.9	−45

[a] Electrochemically induced in acetonitrile solution with 0.6 M $TBAPF_6$ as supporting electrolyte; average temperature of the data range $T=$ 284.8 K. [b] Base-induced formation of the deprotonated isomer with MeO^-Na^+ in methanol solution; average temperature of the data range $T=302.3$ K. [c] $E_a=\Delta H^{\neq}+RT$. [d] $A=(k_BT/h)\exp(1+\Delta S^{\neq}/R)$. [e] Data from ref. [35].

ure 1e). At the highest scan rates the isomerization steps cannot occur before the electron-transfer reactions are reversed, and the voltammograms show the simple waves of a single $Ru^{III/II}$ couple (Figure 1d). Depending on the initial scan direction, these reversible waves can be attributed to either the N_6 or to the N_5O isomer, and the half-wave potentials for the two isomeric forms can be directly determined under these conditions. Both isomerization equilibria are essentially completely on the side of the $Ru^{II}N_6$ or the $Ru^{III}N_5O$ isomer, as evidenced by the absence of voltammetric peaks from the reduction of $Ru^{III}N_6$ or oxidation of the $Ru^{II}N_5O$ isomer at the lower scan rate where the isomerizations approach equilibrium. Only at very low scan rate (0.010 V s^{-1}) does the effect of the reverse reaction ($Ru^{III}N_5O\rightarrow Ru^{III}N_6$) become noticeable, in the form of a minor reduction peak from $Ru^{III}N_6$ due to equilibration during the voltammetric scan (see Supporting Information). Simulations of this feature result in an estimate of 2×10^2 for K_{III}. Isomerization in the Ru^{II} state is for practical purposes irreversible with K_{II} on the order of 10^6, which follows from the other square-scheme parameters as thermodynamically superfluous ($\ln(K_{II}K_{III})=\{E_{1/2}(N_6)-E_{1/2}(N_5O)\}F/RT$).

The isomerization rate constants are considerably temperature dependent, as shown by comparing voltammograms recorded at temperatures between −30 and +45 °C (Figure 2a–c). At a constant scan rate of 50 V s^{-1} isomerization is almost totally suppressed at the lowest temperature, while complete isomerization is observed at the highest temperature. Rate constants as a function of temperature were obtained from digital simulations for a range of scan rates for each temperature. The activation energies E_a and pre-exponential factors A were obtained from Arrhenius plots (Figure 2d) and are compiled in Table 2 together with the enthalpies and entropies of activation $\Delta H^{\neq}$ and $\Delta S^{\neq}$, which were obtained from E_a and A, respectively (see also the Supporting Information). The values of E_a are similar for electrochemically induced isomerization in both oxidation states but are smaller than E_a for the chemically induced isomerization that occurs in the Ru^{II} state in the presence of strong bases and results in the deprotonated N_5O isomer.[35,41] All isomerization reactions have negative activation entropies of similar magnitude. For the unimolecular isomerizations the negative values of $\Delta S^{\neq}$ indicate that the

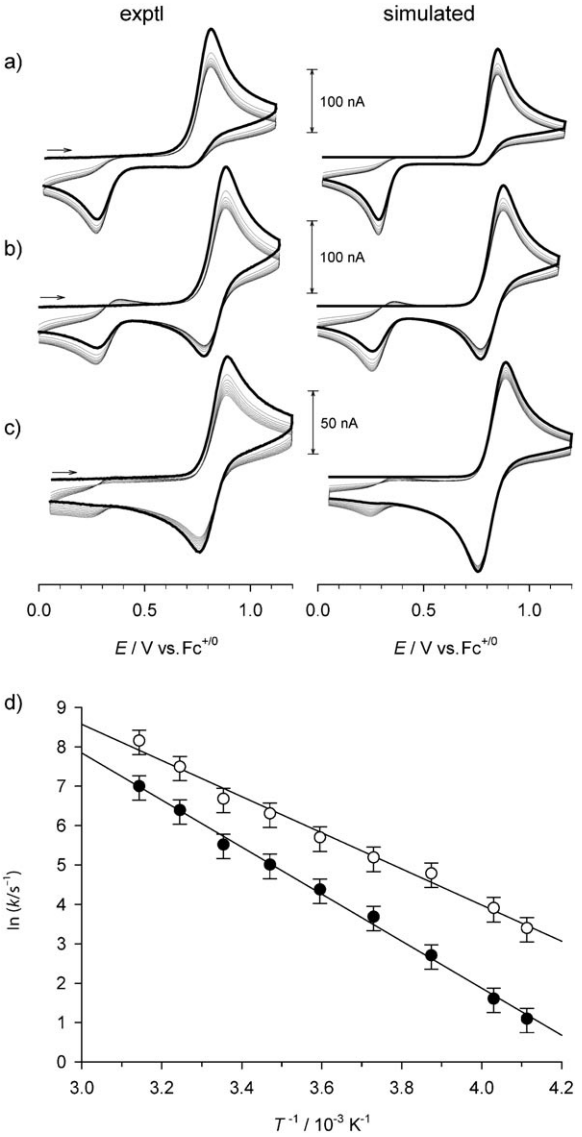

Figure 2. Experimental and simulated voltammograms (50 V s^{-1}) of **1** (6 mM) in acetonitrile with 0.6 M $TBAPF_6$ at a) 45, b) 5, and c) −30 °C. Scan 1 (thick line) and scans 2–10 (thin lines) at a Pt microdisk electrode (∅ 25 μm). (d) Arrhenius plots for k_{II} (○) and k_{III} (●).

transition states are characterized by reduced degrees of freedom in the form of restricted vibrations or internal rotations of the complex. The computational results (see below) suggest that such constraints could arise when the methyl substituent of the ambidentate ligand must rotate along the pyridine ring during isomerization.

For further development of molecular switches based on the principal motif of **1**, it would be essential to identify structural parameters that govern the rate and equilibrium constants of the isomerization reactions. The two obvious parameters are 1) steric effects that could hinder rotation of the ambidentate unit and 2) electronic effects that could influence the extent to which the Ru^{II} and Ru^{III} oxidation states prefer the N_6 and N_5O ligand sets, respectively.

Steric effects: Complexes **2**–**4** were studied to infer the extent to which steric hindrance around the hinge of the molecular switch affects isomerization. For this purpose substituents of different steric bulk were placed on the carbon atom linking the rotating unit of the ambidentate ligand with its stationary bipyridyl unit.

For the phenyl-substituted complex **3** the voltammetric response is qualitatively identical to that of methyl analogue **1**. Both isomerization rates are, however, drastically reduced compared to **1**, while the equilibrium constants for **3** are also largely on the side of the $Ru^{II}N_6$ and $Ru^{III}N_5O$ isomers when the complex is in its Ru^{II} and Ru^{III} state, respectively (Table 1).

For complex **4** with the even bulkier *tert*-butyl substituent, a simple quasireversible wave at $E_{1/2}=0.81$ V was observed even for the lowest scan rate (0.01 $V s^{-1}$), that is, no signs of isomerization could be observed on the voltammetry timescale, which puts an upper limit of $k_{III}<10^{-3}\,s^{-1}$ on the isomerization rate constant. However, when the $Ru^{III}N_6$ complex was generated by exhaustive electrolysis at 0.92 V its slow isomerization could be followed on a timescale of 10^3 s. Figure 3 shows voltammograms of the electrolyzed solution that monitored the decreasing reduction peaks arising from the $Ru^{III}N_6$ complex ($E_{pc}=0.77$ V) and the emerging peak from the $Ru^{III}N_5O$ isomer ($E_{pc}=$ 0.20 V) for more than one hour. Plots of peak currents versus time are exponential with an observed rate constant of $k_{obs}=7.3\times10^{-4}\,s^{-1}$. Since isomerization does not go to completion ($K_{III}=k_{III}/k_{-III}=2.7$) the contribution of the reverse reaction to the observed rate constant ($k_{obs}=k_{III}+k_{-III}$) must be taken into account; this results in $k_{III}=5.3\times10^{-4}\,s^{-1}$. However, the $Ru^{II}N_5O\rightarrow Ru^{II}N_6$ isomerization is significantly faster, as indicated by the ratio of voltammetric peak currents ($i_{pa}/i_{pc}<1$) for the $Ru^{III/II}$ wave of the N_5O isomer (Figure 3). From comparison of the last voltammogram in Figure 3 to digital simulations, a value of k_{II} on the order of 0.1 s^{-1} was estimated.

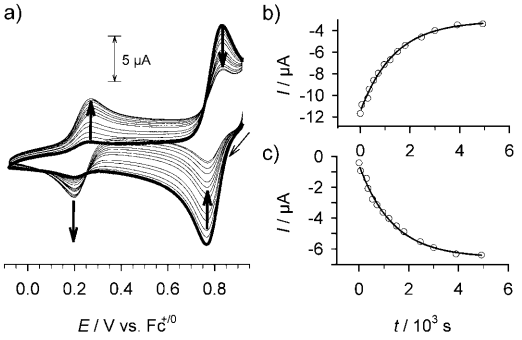

Figure 3. a) Voltammograms (0.1 $V s^{-1}$) of **4** (1 mM) in acetonitrile with 0.1 M $TBAPF_6$ on a glassy carbon electrode (∅3 mm) immediately after exhaustive electrolysis and during the following 80 min (bold arrows indicate direction of changes). Peak current of 0.77 (b) and 0.20 V (c).

The previous results indicate a drastic effect of steric hindrance on the isomerization rates with a difference of six orders of magnitude between the *tert*-butyl- and methyl-substituted ligands. In view of these findings, complex **2** was prepared in which the methyl group of the parent complex was replaced by a hydrogen atom. We anticipated that the isomerization rates of **2** would either exceed those of the methyl analogue due to further decrease of steric hindrance or would be at least comparable if the rates of isomerization in **1** were no longer limited by steric hindrance. Intriguingly, the voltammetric data show no signs of isomerization at all (Figure 4a). Even at the lowest scan rates the simple wave attributable to the reversible $Ru^{III/II}$ couple of the N_6 complex ($E_{1/2}=0.83$ V) was observed, and this imposes an upper limit of $10^{-3}\,s^{-1}$ on k_{III}. No voltammetric wave attributable

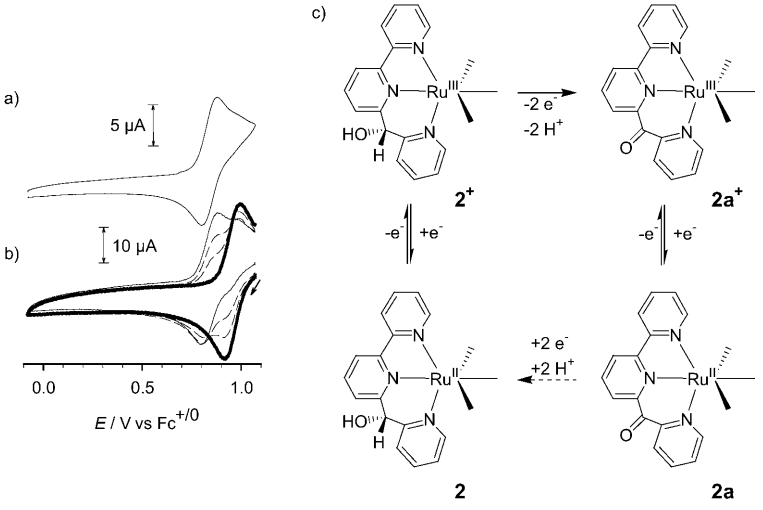

Figure 4. a) Voltammogram (0.1 $V s^{-1}$) of **2** (1 mM) in acetonitrile with 0.1 M $TBAPF_6$. b) Voltammograms (0.2 $V s^{-1}$) before (thin line), during (dashed line) and after (thick line) exhaustive electrolysis at 1.07 V. c) Proposed mechanism of the three-electron oxidation of **2** to $\mathbf{2a}^+$.

to the N_5O isomer could be observed even when the possibility of very slow isomerization of **2** was investigated on a timescale of 10^2–10^4 s by a combination of exhaustive electrolysis and voltammetric product analysis (Figure 4b). Instead, the coulometric data revealed that exhaustive oxidation at 1.07 V is a three-electron process. The product is characterized by a reversible voltammetric wave at $E_{1/2} =$ 0.95 V that corresponds to a one-electron process, as evidenced by coulometry. This half-wave potential of the product species is in exact agreement with the reported data for the $Ru^{III/II}$ couple of keto-functionalized complex **2a**.[38] Hence, we assign the three-electron process observed at 1.07 V to a combination of one-electron oxidation of the metal center with two-electron oxidation of the secondary alcohol function of the ligand that results in formation of $\mathbf{2a}^+$ (Figure 4c). Ligand oxidation is apparently thermodynamically feasible at the potential of the $Ru^{III/II}$ couple of **2** but does not occur on the voltammetric timescale, where a reversible one-electron wave is observed. The sluggishness of ligand oxidation may arise from limitations in deprotonation steps that rely on traces of water as proton acceptor in the carefully dried acetonitrile solution. Reduction of **2a** to **2** required strongly negative potential (<0 V) and did not quantitatively recover **2**.

The relative order of isomerization rates for **1**, **3**, and **4** follows the expected trend (**1**>**3**>**4**) with the size of the substituent R. This effect could be readily rationalized in terms of increased activation energies due to steric hindrance of rotation of the ambidentate unit. Furthermore, it can be envisioned that activation entropies are rendered increasingly negative, and thus pre-exponential factors decrease, as larger substituents with more internal degrees of freedom become sterically constrained in the transition state. The intriguing finding that no isomerization is observed for complex **2** cannot be attributed to kinetic effects related to the size of R, however. We therefore considered the possibility that in the complexes with bulkier substituents a certain amount of strain in the ambidentate ligand destabilizes the N_6 isomer and thereby renders isomerization thermodynamically favorable if it is at least partly released in this process. The notion of distorted coordination geometries due to bulkier substituents was corroborated by DFT calculations with Gaussian 03 at the B3LYP/3-21G* level of theory.[42] The gas-phase optimized geometries of the $Ru^{III}N_6$ forms of **1**–**4** revealed significant differences in the degree of distortion away from the ideal coordination geometry of the pyridyl group in the ambidentate ligand (see the Supporting Information). Within our series of complexes the degree of distortion is ordered as **2**<**3**<**1**<**4**, where the unexpectedly low amount of strain in **3** is due to the ability of the phenyl group to rotate so as to minimize its steric effect on, and possibly create edge-to-face π–π stacking with, the adjacent pyridine ring. The computational studies provided additional insight into the isomerization process in the form of one-dimensional potential-energy surfaces. These were calculated by rotating the ambidentate unit about the bond connecting it to the stationary bipyridine moiety. For simplicity, only the atoms in the rotating part of the ambidentate ligand are free to move during this process, so that the resulting potential-energy surface only offers a qualitative description of the isomerization process. For complex **1**, the surface shows two maxima (Figure 5), the first of which, after a rotation of about 33°, occurs when the methyl substituent passes across the edge of the bipyridine moiety (peak B). The nitrogen atom remains bound to the ruthenium center until the oxygen atom is close enough to bind, and the second barrier (C) occurs when the ruthenium center actually changes ligand, which also causes the proton on the oxygen atom to transfer to the nitrogen atom. Figure 5 thus indicates that the rate of isomerization in this type of complexes could in principle depend on two distinct parameters: steric hindrance to rotation of R across the bipyridine moiety and the barrier to ligand exchange. For complex **4** the potential-energy surface (Supporting Information) shows an even more pronounced activation barrier associated with the increased steric hindrance to rotation, which should be the rate-limiting step in the very slow isomerization of this complex. For complex **2**, on the other hand, the dominant barrier arises from the ligand-exchange step, and the overall process provides no or little stabilization within the framework of these calculations (see the Supporting Information). In summary, it appears that the size of R not only determines the barrier to rotation but it also affects the coordination geometry of the ambidentate ligand. The latter effect could lie behind the unexpected behavior of **2**, which is least strained in the N_6 form and seems to suffer from a lack of driving

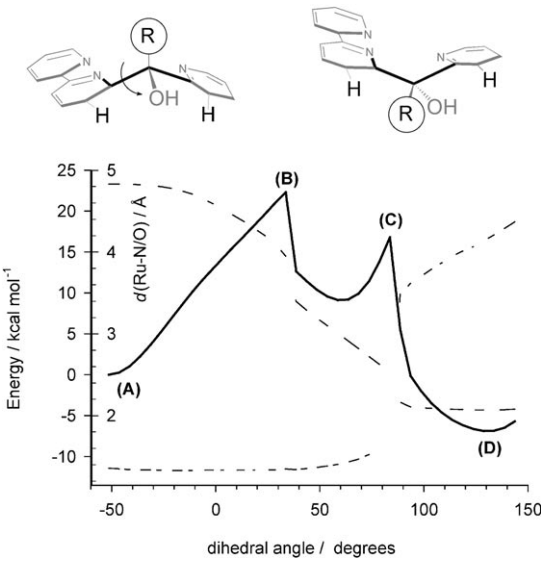

Figure 5. Schematic view of the ambidentate ligand in the N_6 form (top left) and during isomerization (top right). Calculated energy (continuous), Ru–N distance (dashes), and Ru–O distance (dot dash) as a function of dihedral angle (defined by the black bonds) describing the isomerization of $Ru^{III}N_6$ (A) to $Ru^{III}N_5O$ (D) for complex **1** (bottom). Schematic structures correspond to (A) and (C). See Supporting Information for the computed structures of (A)–(D).

force and a high activation barrier for the actual ligand-exchange step as compared to the more strained analogues.

Electronic effects: It could be anticipated that electron-withdrawing substituents on the spectator ligand should increase the preference of the Ru^{III} state for the O-donor function of the ambidentate ligand, while electron-donating substituents should render N coordination more favorable. Such effects could be used to tune the equilibrium constants and possibly also rate constants of the isomerization reactions. In complexes **5**–**8** we therefore replaced the *p*-tolyl substituent on the terpyridyl ligand of the parent complex by a range of substituents with different electronic properties. The relative extent of electron-donating or -withdrawing effects experienced by the metal center can be inferred from the half-wave potentials of the $Ru^{III/II}$ couples. For ester-substituted complex **5** the potentials of the $Ru^{III/II}$ couples in both isomers are almost identical to the parent complex and the rate and equilibrium constants are accordingly very similar between **1** and **5**. The strongly electron withdrawing ester substituent is not in direct conjugation with the terpyridyl ligand, which explains its small electronic effect on the switching behavior. In case of complex **6** the electron-withdrawing effect of the chloro substituent creates a small but significant anodic shift of the potentials. The rate and equilibrium constants are, however, very similar to those of parent complex **1**. Likewise, the weak electron-donating effect of the alkoxyl substituent in complex **7** results only in minor effects on the isomerization reactions. However, the expected effect on the equilibria, in the form of a reduced K_{III} and increased K_{II}, is evident. More substantial effects on the isomerization reactions were only brought about by the strongly electron donating pyrrolidine substituent of complex **8**. Here the electron deficiency of the Ru^{III} state is balanced by the pyrrolidine group to an extent that the rate and equilibrium constant for isomerization to the N_5O form are reduced by one order of magnitude. As a consequence, the voltammetric responses of **7** and **8** differ from those of the other complexes in the sense that the reverse peak for the $Ru^{III/II}N_6$ couple, that is, reduction of the $Ru^{III}N_6$ isomer, occurs not only at high scan rates but also becomes very prominent at low scan rates (Figure 6). The latter effect is due to equilibration between $Ru^{III}N_6$ and $Ru^{III}N_5O$ that regenerates $Ru^{III}N_6$ as it is consumed during the voltammetric scan.

An additional effect of the pyrrolidine substituent is the unusual electrochromic behavior of complex **8** (Figure 7). In the Ru^{II} state all complexes feature an intense MLCT band around 480 nm that is typical for the Ru polypyridyl motif and results in the orange to red color of the reduced state of all complexes (Table 3 and the Supporting Information).

Oxidation to the Ru^{III} state results in bleaching of the MLCT band and renders the oxidized complexes essentially colorless or pale yellow in dilute solution. However, in case of complex **8** the Ru^{III} state features a pronounced band peaking at 670 nm. This absorption can be tentatively attributed to a ligand-to-metal charge-transfer (LMCT) transition between the pyrrolidine-substituted terpyridine ligand and the Ru^{III} center of the $Ru^{III}N_5O$ complex and endows solutions of the oxidized complex with a distinct green color.

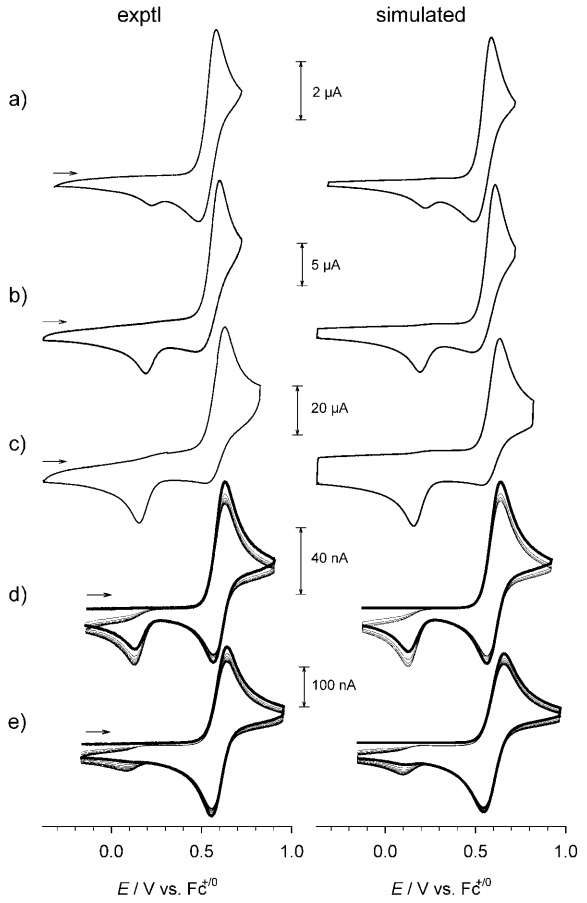

Figure 6. Cyclic voltammograms of **8** in acetonitrile (left) and digital simulations with the parameters from Table 1 (right). a–c) Scan 1 for a 1 mM solution with 0.1 M $TBAPF_6$ on glassy carbon electrode (∅ 3 mm). d, e) Scan 1 (thick line) and scans 2–10 (thin lines) for 6 mM solution with 0.6 M $TBAPF_6$ on a Pt microdisk electrode (∅25 μm). Scan rates: 0.01 $V s^{-1}$ (a), 0.1 $V s^{-1}$ (b), 1 $V s^{-1}$ (c), 10 $V s^{-1}$ (d), 100 $V s^{-1}$ (e).

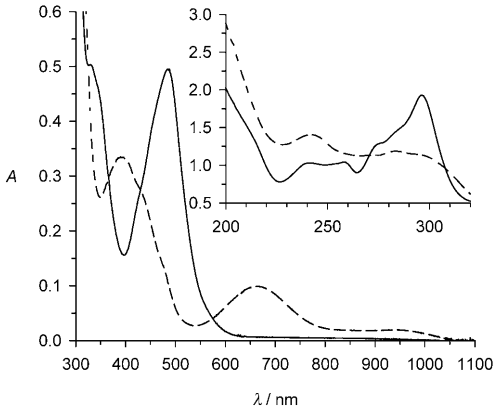

Figure 7. Electronic absorption spectrum of **8** (0.38 mM) (continuous line) and product spectrum after oxidation at 0.72 V (dashed line) in acetonitrile solution. $[Ru^{III}N_5O]/[Ru^{III}N_6] = 12$ (see Table 1).

Table 3. Electronic absorption spectroscopic data in acetonitrile solution[a] at 298 K.

Compd[b]	$Ru^{II}N_6$, λ_{max} (ε)[c] [nm (10^4 M^{-1} cm^{-1})]	$Ru^{III}N_5O$, λ_{max} (ε)[c] [nm] (10^4 M^{-1} cm^{-1})]
1[d]	420 (sh), 482 (1.4), 540 (sh), 600 (sh)	410 (sh), 540 (sh)
2	472 (ca. 1.3)[e]	–[f]
3	420 (sh), 484 (1.4), 540 (sh), 600 (sh)	390 (1.0), 540 (sh)
4	420 (sh), 480 (1.5), 540 (sh), 600 (sh)	–[g]
5	420 (sh), 483 (1.4), 550 (sh), 610 (sh)	–[g]
6	420 (sh), 475 (1.0), 550 (sh), 610 (sh)	393 (0.5), 520 (sh)
7	420 (sh), 474 (1.1), 580 (sh)	382 (6.2), 520 (sh)
8	487 (1.3)	395 ($\approx$0.9),[h] 665 ($\approx$0.3),[h] ca. 950[i]

[a] With 0.1 M (n-$C_4H_9)_4NPF_6$ as supporting electrolyte. [b] As PF_6^- salts. [c] Peaks and pronounced shoulders in the visible range. [d] Data from ref. [35]. [e] Extinction coefficient less accurate due to contamination with **2a**. [f] Not observed. [g] Not measured. [h] Extinction coefficient less accurate due to incomplete isomerization. [i] Possibly due to residual $Ru^{III}N_6$ isomer.

The minor band with a maximum around 900–950 nm is about 0.5 eV lower in energy and presumably arises from the corresponding LMCT transition of the $Ru^{III}N_6$ isomer that constitutes about 8% of the oxidized complex.[43]

Conclusion

Our concept of a ligand-bound ambidentate motif for electron-transfer-induced linkage isomerization offers a general approach to bistable molecular switches in the form of Ru polypyridyl complexes. The switching characteristics can be tuned over a wide range by means of substituents on the ligands.

The effect of substituents on the ambidentate unit demonstrates that steric hindrance to rotational ligand rearrangement can severely restrict the rates of isomerization. On the other hand, it could be shown that the size of the substituent also affects the coordination geometry and that the H-substituted complex, which is the least distorted in the N_6 isomer, does not isomerize to the N_5O isomer despite having minimum steric hindrance to rotation. This makes the originally used methyl group still the most advantageous for applications aiming at maximum isomerization rates.

Substituents on the spectator ligand interfere little with isomerization reactions as long as the electron-donating or -withdrawing effects are modest. Substituents with substantially stronger electron-withdrawing effect would be required to significantly destabilize the $Ru^{III}N_6$ isomer. The donor substituents in our series prove, however, that substituents on the spectator ligand indeed can affect the preference of the metal center for different binding modes of the ambidentate ligand and can be used to tune rates and equilibrium constants. Overall, the results demonstrate that rational selection of anchoring or linking groups for immobilization or incorporation in larger molecular assemblies will not interfere detrimentally with isomerization, which is important in view of future applications of the molecular switches.

Experimental Section

General: All reagents and solvents were used as received, except THF and diethyl ether, which were distilled from sodium/benzophenone prior to use. 2,2-Dimethyl-1-(2-pyridyl)-propanone was prepared as described by Nordström et al.[44] The compounds 4′-(*p*-tolyl)-2,2′:6′,2″-terpyridine (ttpy),[45] 4′-(4-methylbenzoate)-2,2′:6′,2″-terpyridine (MeO_2CPh-tpy),[46] 4′-chloro-2,2′:6′,2″-terpyridine (Cl-tpy),[47] 4′-ethoxy-2,2′:6′,2″-terpyridine (EtO-tpy),[47] 1-[6-(2,2′-bipyridyl)]-1-(2-pyridyl)ethanol (L-Me-OH),[38] [Ru(L-Me-OH)(ttpy)]$(PF_6)_2$ (**1**),[38] [Ru(L-Ph-OH)(ttpy)]$(PF_6)_2$ (**3**),[36] and [Ru(L-Me-OH)(*N*Pyr-tpy)]$(PF_6)_2$ (**8**)[48] were synthesized according to literature procedures. The ruthenium(II) precursors [$RuCl_2$(dmso)(ttpy)], [$RuCl_2$(Cl-tpy)(dmso)], [$RuCl_2$(dmso)(EtO-tpy)], and [$RuCl_2$(dmso)(MeO_2CPh-tpy)] were prepared from [$RuCl_2(dmso)_4$] and the appropriate 2,2′:6′,2″-terpyridyl ligand, as described by Ziessel and co-workers.[39] The obtained compounds were used without further purification. Microwave heating was performed in an Initiator single-mode microwave cavity at 2450 MHz (Biotage). ^{1}H NMR were recorded on Varian 300 MHz or 400 MHz or JEOL 400 MHz spectrometers at 293 K, and UV/Vis absorption spectra were measured on a Varian Cary 50 spectrophotometer. HPLC-MS data were obtained on a Dionex Ultimate 3000 system on a Phenomenex Gemini C18 column (150×3.0 mm, 5 μm) coupled to a Thermo LCQ Deca XP with electrospray ionization (ESI). Solvents used for HPLC: 0.05% HCO_2H in H_2O and 0.05% HCO_2H in CH_3CN.

6-(2,2′-Bipyridyl)-2-pyridyl-methanol (L-H-OH): 6-Bromo-2,2′-bipyridine (0.300 g, 1.28 mmol) was dissolved in THF/Et_2O (1/4, 10 mL) under a nitrogen atmosphere. The temperature was reduced to −78 °C. *n*BuLi (2.5 M in hexanes, 0.55 mL, 1.4 mmol) was added dropwise and the dark red solution was left to stir for 15 min. 2-Pyridinecarboxaldehyde (0.14 mL, 1.5 mmol) was added dropwise and the mixture was warmed to room temperature. Saturated NH_4Cl was added and the mixture extracted with Et_2O. The organic phase was dried over Na_2SO_4, the solvent was removed, and the residue purified by chromatography on silica (eluent: pentane/EtOAc 2/1) to give **L-H-OH** (0.214 g, 64%). ^{1}H NMR ($CDCl_3$): δ = 5.93 (d, 1H), 5.98 (d, 1H), 7.19 (ddd, 1H), 7.32 (ddd, 1H), 7.55 (m, 1H), 7.60 (m, 1H), 7.65 (dt, 1H), 7.78 (t, 1H), 7.84 (dt, 1H), 8.31 (m, 1H), 8.48 (m, 1H), 8.57 (m, 1H), 8.68 ppm (m, 1H); ^{13}C NMR ($CDCl_3$): δ = 75.5, 120.1, 121.3, 121.4, 121.5, 122.9, 124.0, 137.0, 137.1, 138.1, 148.4, 149.4, 154.7, 155.9, 160.3, 161.1 ppm; LC-MS (EI): m/z 264.2 $[M+H]^+$ (calcd 264.1).

1-[6-(2,2′-Bipyridyl)]-2,2-dimethyl-1-(2-pyridyl)propanol (L-*t*Bu-OH). The compound was prepared as above. 6-Bromo-2,2′-bipyridine (0.102 g, 0.43 mmol), *n*BuLi (2.5 M in hexanes, 0.2 mL, 0.5 mmol), and 2,2-dimethyl-1-(2-pyridyl)-propanone (0.074 g, 0.45 mmol) in THF/Et_2O (1/4, 7 mL) gave **L-*t*Bu-OH** (0.045 g, 33%). ^{1}H NMR ($CDCl_3$): δ = 1.07 (s, 9H), 7.06 (s, 1H), 7.20 (ddd, 1H), 7.34 (ddd, 1H), 7.68 (m, 1H), 7.82 (t, 1H), 7.89 (dt, 1H), 8.25 (dd, 1H), 8.30–8.38 (m, 2H), 8.45 (m, 1H), 8.56 (m, 1H), 8.71 ppm (m, 1H); ^{13}C NMR ($CDCl_3$): δ = 26.6, 41.1, 80.9, 119.4, 121.1, 122.2, 123.8, 124.0, 124.2, 135.9, 137.2, 137.3, 146.5, 149.4, 153.3, 156.6, 161.4, 162.2 ppm; LC-MS (EI): m/z 320.3 $[M+H]^+$ (calcd 320.2).

[Ru(ttpy)(L-H-OH)]$(PF_6)_2$ (2): [$RuCl_2$(dmso)(ttpy)] (0.108 g, 0.19 mmol) and L-H-OH (0.054 g, 0.20 mmol) were heated by microwave in argon-degassed EtOH/H_2O (2/1, 15 mL) at 140 °C for 60 min. The solvent was removed and the crude product purified by chromatography on silica (eluent: CH_3CN/H_2O/satd. KNO_3 mixtures). A minor purple fraction corresponding to oxidation product **2a** was eluted somewhat slower than major product **2**. The solvent was removed, and the remaining solid redissolved in H_2O/acetone (1/1). Saturated aqueous NH_4PF_6 was added, and

the resulting precipitate was filtered off and washed with H_2O and Et_2O (0.128 g, 69%). ^1H NMR (400 MHz, CD_3CN, 25°C): $\delta = 2.53$ (s, 3H), 5.13 (s, 1H), 6.29 (s, 1H), 6.89 (m, 1H), 6.96 (m, 1H), 7.05–7.12 (m, 2H), 7.28–7.36 (m, 3H), 7.57 (d, 2H), 7.73 (m, 1H), 7.81 (m, 1H), 7.88 (m, 1H), 7.94–8.04 (m, 2H), 8.09 (d, 2H), 8.18 (d, 1H), 8.35–8.44 (m, 3H), 8.54 (d, 1H), 8.58–8.66 (m, 2H), 8.92 ppm (s, 2H); ESIMS: m/z: 832.9 $[M-PF_6^-]^+$ (calcd for $C_{38}H_{30}N_6ORuPF_6$: 833.1), 344.2 $[M-2PF_6^-]^{2+}$ (calcd for $C_{38}H_{30}N_6ORu$: 344.1). Complex **2a** could be readily identified as the only component after dissolving in air-equilibrated CH_3CN (ca. 10^{-5} M) by ESIMS: m/z: 830.9 $[M-PF_6^-]^+$ (calcd for $C_{38}H_{28}N_6ORuPF_6$: 830.7), 343.3 $[M-2PF_6^-]^{2+}$ (calcd for $C_{38}H_{28}N_6ORu$: 343.1).

General procedure for preparation of ruthenium(II) complexes 4–7: The precursors $[RuCl_2(dmso)(Y\text{-tpy})]$and L-X-OH were added to EtOH/H_2O (2/1, 5–10 mM solutions). The mixture was degassed and heated to reflux under an argon atmosphere (15–24 h). The solvent was removed and the residue purified by chromatography on silica (eluent: CH_3CN/H_2O/satd. KNO_3 mixtures). Fractions containing product were combined, the solvent removed, and the remaining solid redissolved in H_2O/acetone (1/1). Saturated aqueous NH_4PF_6 was added, and the resulting precipitate was filtered off and washed with H_2O and Et_2O.

[Ru(ttpy)(L-*t*Bu-OH)](PF$_6$)$_2$ (4): Yield: 37%. ^1H NMR (CD_3CN): $\delta =$ 0.73 (s, 9H), 2.53 (s, 3H), 5.43 (s, 1H), 6.87 (m, 1H), 6.90 (m, 1H), 7.04 (m, 1H), 7.10 (m, 1H), 7.14 (m, 1H), 7.31 (m, 1H), 7.46 (dd, 1H), 7.55–7.64 (m, 3H), 7.75–7.83 (m, 2H), 8.05 (dt, 1H), 8.07–8.18 (m, 4H), 8.32 (d, 1H), 8.39 (d, 1H), 8.42 (d, 1H), 8.68 (dd, 1H), 8.73 (m, 1H), 8.75 (d, 1H), 8.81 (dd, 1H), 9.04 ppm (d, 1H); ESIMS: m/z: 888.7 $[M-PF_6^-]^+$ (calcd for $C_{42}H_{38}N_6ORuPF_6$: 889.2), 372.0 $[M-2PF_6^-]^{2+}$ (calcd for $C_{42}H_{38}N_6ORu$: 372.1); elemental analysis (%) calcd for $C_{42}H_{38}N_6ORuP_2F_{12}\cdot H_2O$: C 47.96, H 3.83, N 7.99; found: C 47.67, H 4.18, N 8.04.

[Ru(MeO$_2$CPh-tpy)(L-Me-OH)](PF$_6$)$_2$ (5): Yield: 46%. ^1H NMR (CD_3CN): $\delta = 1.81$ (s, 3H), 4.00 (s, 3H), 5.21 (s, 1H), 6.90 (m, 1H), 6.95 (d, 1H), 7.06–7.12 (m, 2H), 7.18 (d, 1H), 7.35 (m, 1H), 7.41 (dd, 1H), 7.71 (dt, 1H), 7.81 (dt, 1H), 7.86 (dt, 1H), 8.00–8.10 (m, 2H), 8.19 (dd, 1H), 8.31 (d, 2H), 8.35–8.40 (m, 3H), 8.44 (t, 1H), 8.50 (d, 1H), 8.64 (dd, 1H), 8.69 (d, 1H), 8.77 (dd, 1H), 8.92 (d, 1H), 9.01 ppm (d, 1H); ESIMS: m/z: 890.7 $[M-PF_6^-]^+$ (calcd for $C_{40}H_{32}N_6O_3RuPF_6$: 891.1), 373.1 $[M-2PF_6^-]^{2+}$ (calcd for $C_{40}H_{32}N_6O_3Ru$: 373.1); elemental analysis (%) calcd for $C_{40}H_{32}N_6O_3RuP_2F_{12}\cdot 3H_2O$: C 44.09, H 3.51, N 7.71; found: C 44.33, H 3.48, N 7.88.

[Ru(Cl-tpy)(L-Me-OH)](PF$_6$)$_2$ (6): Yield: 51%. ^1H NMR (CD_3CN): $\delta =$ 1.76 (s, 3H), 5.30 (s, 1H), 6.87–6.95 (m, 2H), 7.05–7.14 (m, 3H), 7.30 (m, 1H), 7.35 (m, 1H), 7.70 (m, 1H), 7.81 (dt, 1H), 7.84 (dt, 1H), 8.01 (dt, 1H), 8.06 (m, 1H), 8.17 (m, 1H), 8.30–8.38 (m, 2H), 8.42 (t, 1H), 8.51 (m, 1H), 8.62 (dd, 1H), 8.72–8.76 (m, 2H), 8.83 ppm (d, 1H). ESIMS: m/z: 790.7 $[M-PF_6^-]^+$ (calcd for $C_{32}H_{25}ClN_6ORuPF_6$: 791.0), 323.1 $[M-2PF_6^-]^{2+}$ (calcd for $C_{32}H_{25}ClN_6ORu$: 323.0); elemental analysis (%) calcd for $C_{32}H_{25}ClN_6ORuP_2F_{12}\cdot H_2O$: C 40.29, H 2.85, N 8.81; found: C 39.96, H 2.70, N 8.89.

[Ru(EtO-tpy)(L-Me-OH)](PF$_6$)$_2$ (7): Yield: 71%. ^1H NMR (CD_3CN): $\delta = 1.64$ (t, 3H), 1.76 (s, 3H), 4.60 (q, 2H), 5.21 (s, 1H), 6.86 (m, 1H), 6.91 (m, 1H), 7.03 (ddd, 1H), 7.11 (m, 1H), 7.19 (m, 1H), 7.29 (ddd, 1H), 7.38 (m, 1H), 7.70 (m, 1H), 7.76–7.83 (m, 2H), 7.98 (dt, 1H), 8.06 (m, 1H), 8.14–8.20 (m, 2H), 8.28 (d, 1H), 8.30–8.37 (m, 2H), 8.38 (t, 1H), 8.52 (m, 1H), 8.60 (dd, 1H), 8.71 ppm (dd, 1H); ESIMS: m/z: $[M-PF_6^-]^+$ 800.7 (calcd for $C_{34}H_{30}N_6O_2RuPF_6$: 801.1); $[M-2PF_6^-]^{2+}$ 328.1 (calcd for $C_{34}H_{30}N_6O_2Ru$: 328.1); elemental analysis (%) calcd for $C_{34}H_{30}N_6O_2RuP_2F_{12}$ (%): C 43.18, H 3.20, N 8.89; found: C 43.72, H 3.84, N 10.05.

Electrochemistry: All electrochemical measurements were performed in acetonitrile solution (Sigma-Aldrich, spectrophotometric grade) dried over 3 Å molecular sieves. Tetrabutylammonium hexafluorophosphate (Fluka, puriss., electrochemical grade) was dried at 80°C in vacuo and was used as supporting electrolyte at concentrations of 0.1 M for standard voltammetry, bulk electrolysis, and spectroelectrochemistry, and 0.6 M for fast voltammetry. All experiments were performed at room temperature unless otherwise specified, and all solutions were deaerated by bubbling with solvent-saturated argon.

Standard voltammetric measurements (0.01–10 $V s^{-1}$) and bulk electrolysis were performed in a three-electrode, three-compartment cell with a glassy carbon disk (∅ 3 mm, CH Instruments, Austin, Texas) or a Pt mesh as working electrode. The reference electrode was a nonaqueous Ag/Ag^+ electrode (10 mM $AgNO_3$ in acetonitrile) with a potential of −0.08 V versus the ferrocenium/ferrocene ($Cp_2Fe^{+/0}$) couple.

Fast voltammetry (10–10000 $V s^{-1}$) was carried out in a custom-built three-electrode cell placed in a Faraday cage. The cell was equipped with a Pt microdisk electrode (∅ 25 μm, CH Instruments Inc., Austin, Texas), a Pt wire counterelectrode, and a Pt wire quasireference electrode (QRE). All potentials measured versus the QRE are referenced to the potential of the $Cp_2Fe^{+/0}$ couple and were determined from measurements with internal ferrocene standard. Temperature in the jacketed cell was controlled between −30 and +45°C by a circulation thermostat bath (Heto, Birkerød, Denmark).

UV/Vis spectroelectrochemical measurements were made with an Agilent 8453 diode-array spectrophotometer. The OTTLE-type quartz cell with an optical path length of 1 mm uses a Pt mesh working electrode and the same reference electrode as described for standard voltammetry.

All electrochemical measurements were performed with an Autolab PGSTAT100 or PGSTAT302 potentiostat controlled with the GPES 4.9 software (ECO Chemie B.V., Utrecht, The Netherlands). The ADC750 fast-sampling A/D converter module (750 kHz) and the SCANGEN analog sweep generator module of the PGSTAT 302 were used for rapid voltammetry. The positive-feedback method implemented in the GPES software was used to determine the approximate ohmic resistance of the cell and to compensate for IR drop. Compensation for most of the resistance (30 kΩ) was applied to all microelectrode measurements and a remainder of 5 kΩ of uncompensated resistance was included in the simulations.

Simulations: Digital simulations of the voltammetric data were performed with the DigiElch 3.0 software (ElchSoft GbR, Kleinromstedt, Germany).[49,50] The half-wave potentials of the $Ru^{III/II}$ couples used for the simulations were determined as averages of the anodic and cathodic peak potentials of the quasireversible waves observed at sufficiently high scan rates where the isomerization reactions are essentially shut down. For the $Ru^{III/II}N_5O$ couple these data were obtained after exhaustive bulk electrolysis or several seconds of equilibration (in case of the ultra micro electrodes) at oxidative potentials (with respect to the $Ru^{III/II}N_6$ couple) that prepared the complex in the $Ru^{III}N_5O$ form. Heterogeneous rate constants were adjusted to a value of 0.15 $cm s^{-1}$ that reproduced the observed scan-rate dependence of the peak separations with the symmetry factor taken as $\alpha = 0.5$ for all electron-transfer reactions. Equal diffusion coefficients (1×10^{-5} $cm^2 s^{-1}$) were used for all species. The non-faradaic background current was approximated in the simulations as a constant charging current arising from a double-layer capacitance of 100 pF.

The rate and equilibrium constants of the isomerization reactions were then adjusted such as to reproduce the heights of the voltammetric peaks and their changes on repeated cycling for the full range of scan rates. In this way a unique set of three independent parameters (k_{II}, k_{III}, K_{III}) and one thermodynamically superfluous parameter (K_{II}) was obtained for each complex.

Acknowledgements

This work was financially supported by the Swedish Energy Agency, the Knut and Alice Wallenberg Foundation, the Carl Trygger Foundation and NEST-STRP, SOLAR-H (EU Contract 516510).

[1] B. L. Feringa, *J. Org. Chem.* **2007**, *72*, 6635–6652.
[2] A. Carella, C. Coudret, G. Guirado, G. Rapenne, G. Vives, J.-P. Launay, *Dalton Trans.* **2007**, 177–186.
[3] S. Saha, J. F. Stoddart, *Chem. Soc. Rev.* **2007**, *36*, 77–92.
[4] C. A. Nijhuis, B. J. Ravoo, J. Huskens, D. N. Reinhoudt, *Coord. Chem. Rev.* **2007**, *251*, 1761–1780.

[5] L. Bogani, W. Wernsdorfer, *Nat. Mater.* **2008**, *7*, 179–186.
[6] J. E. Green, J. W. Choi, A. Boukai, Y. Bunimovich, E. Johnston-Halperin, E. DeIonno, Y. Luo, B. A. Sheriff, K. Xu, Y. S. Shin, H.-R. Tseng, J. F. Stoddart, J. R. Heath, *Nature* **2007**, *445*, 414–417.
[7] U. Kölle, *Angew. Chem.* **1991**, *103*, 970–972.
[8] J. Zarembowitch, O. Kahn, *New J. Chem.* **1991**, *15*, 181–190.
[9] The term bistability is used here in the sense of a hysteresis-like behavior.
[10] K. T. Potts, M. Keshavarz-K, F. S. Tham, H. D. Abruna, C. R. Arana, *Inorg. Chem.* **1993**, *32*, 4422–4435.
[11] V. Amendola, C. Mangano, P. Pallavicini, M. Zema, *Inorg. Chem.* **2003**, *42*, 6056–6062.
[12] V. Amendola, L. Fabbrizzi, P. Pallavicini, *Coord. Chem. Rev.* **2001**, *216–217*, 435–448.
[13] V. Amendola, L. Fabbrizzi, L. Gianelli, C. Maggi, C. Mangano, P. Pallavicini, M. Zema, *Inorg. Chem.* **2001**, *40*, 3579–3587.
[14] R. Ballardini, V. Balzani, A. Credi, M. T. Gandolfi, M. Venturi, *Acc. Chem. Res.* **2001**, *34*, 445–455.
[15] P. R. Ashton, R. Ballardini, V. Balzani, A. Credi, K. R. Dress, E. Ishow, C. J. Kleverlaan, O. Kocian, J. A. Preece, N. Spencer, J. F. Stoddart, M. Venturi, S. Wenger, *Chem. Eur. J.* **2000**, *6*, 3558–3574.
[16] B. Champin, P. Mobian, J.-P. Sauvage, *Chem. Soc. Rev.* **2007**, *36*, 358–366.
[17] V. Balzani, A. Credi, S. Silvi, M. Venturi, *Chem. Soc. Rev.* **2006**, *35*, 1135–1149.
[18] S. Angelos, Y.-W. Yang, K. Patel, J. F. Stoddart, J. I. Zink, *Angew. Chem.* **2008**, *120*, 2254–2258; *Angew. Chem. Int. Ed.* **2008**, *47*, 2222–2226.
[19] S. Angelos, E. Johansson, J. F. Stoddart, J. I. Zink, *Adv. Funct. Mater.* **2007**, *17*, 2261–2271.
[20] S. Saha, K. C. F. Leung, T. D. Nguyen, J. F. Stoddart, J. I. Zink, *Adv. Funct. Mater.* **2007**, *17*, 685–693.
[21] H. Higuchi, E. Ohta, H. Kawai, K. Fujiwara, T. Tsuji, T. Suzuki, *J. Org. Chem.* **2003**, *68*, 6605–6610.
[22] J.-I. Nishida, T. Suzuki, M. Ohkita, T. Tsuji, *Angew. Chem.* **2001**, *113*, 3351–3354; *Angew. Chem. Int. Ed.* **2001**, *40*, 3251–3254.
[23] T. Suzuki, J.-i. Nishida, T. Tsuji, *Chem. Commun.* **1998**, 1331–1332.
[24] T. Suzuki, M. Kondo, T. Nakamura, T. Fukushima, T. Miyashi, *Chem. Commun.* **1997**, 2325–2326.
[25] T. Suzuki, J.-i. Nishida, T. Tsuji, *Angew. Chem.* **1997**, *109*, 1387–1389; *Angew. Chem. Int. Ed. Engl.* **1997**, *36*, 1329–1331.
[26] E. Ohta, H. Higuchi, H. Kawai, K. Fujiwara, T. Suzuki, *Org. Biomol. Chem.* **2005**, *3*, 3024–3031.
[27] M. Sano, *Struct. Bonding (Berlin)* **2001**, *99*, 117–139.
[28] A. Tomita, M. Sano, *Inorg. Chem.* **2000**, *39*, 200–205.
[29] M. Sano, H. Taube, *Inorg. Chem.* **1994**, *33*, 705–709.
[30] A. A. Rachford, J. L. Petersen, J. J. Rack, *Inorg. Chem.* **2006**, *45*, 5953–5960.
[31] J. J. Rack, A. A. Rachford, A. M. Shelker, *Inorg. Chem.* **2003**, *42*, 7357–7359.
[32] J. J. Rack, N. V. Mockus, *Inorg. Chem.* **2003**, *42*, 5792–5794.
[33] J. J. Rack, J. R. Winkler, H. B. Gray, *J. Am. Chem. Soc.* **2001**, *123*, 2432–2433.
[34] T. Hamaguchi, K. Ujimoto, I. Ando, *Inorg. Chem.* **2007**, *46*, 10455–10457.
[35] O. Johansson, R. Lomoth, *Chem. Commun.* **2005**, 1578–1580.
[36] O. Johansson, R. Lomoth, *Inorg. Chem.* **2008**, *47*, 5531–5533.
[37] G. Tsekouras, N. Minder, E. Figgemeier, O. Johansson, R. Lomoth, *J. Mater. Chem.* **2008**, *18*, 5824–5829.
[38] M. Abrahamsson, H. Wolpher, O. Johansson, J. Larsson, M. Kritikos, L. Eriksson, P.-O. Norrby, J. Bergquist, L. Sun, B. Åkermark, L. Hammarström, *Inorg. Chem.* **2005**, *44*, 3215–3225.
[39] R. Ziessel, V. Grosshenny, M. Hissler, C. Stroh, *Inorg. Chem.* **2004**, *43*, 4262–4271.
[40] Due to the improved data quality the potentials and rate constants given here for complex **1** are more accurate than the previously reported values.
[41] In its deprotonated form complex **1** is locked in the N_5O isomer independent of oxidation state, in analogy to the "write-protection" mechanism later reported by Hamaguchi and co-workers.[34]
[42] Gaussian 03, Revision C.02, M. J. Frisch, G. W. Trucks, H. B. Schlegel, G. E. Scuseria, M. A. Robb, J. R. Cheeseman, J. A. Montgomery, Jr., T. Vreven, K. N. Kudin, J. C. Burant, J. M. Millam, S. S. Iyengar, J. Tomasi, V. Barone, B. Mennucci, M. Cossi, G. Scalmani, N. Rega, G. A. Petersson, H. Nakatsuji, M. Hada, M. Ehara, K. Toyota, R. Fukuda, J. Hasegawa, M. Ishida, T. Nakajima, Y. Honda, O. Kitao, H. Nakai, M. Klene, X. Li, J. E. Knox, H. P. Hratchian, J. B. Cross, V. Bakken, C. Adamo, J. Jaramillo, R. Gomperts, R. E. Stratmann, O. Yazyev, A. J. Austin, R. Cammi, C. Pomelli, J. W. Ochterski, P. Y. Ayala, K. Morokuma, G. A. Voth, P. Salvador, J. J. Dannenberg, V. G. Zakrzewski, S. Dapprich, A. D. Daniels, M. C. Strain, O. Farkas, D. K. Malick, A. D. Rabuck, K. Raghavachari, J. B. Foresman, J. V. Ortiz, Q. Cui, A. G. Baboul, S. Clifford, J. Cioslowski, B. B. Stefanov, G. Liu, A. Liashenko, P. Piskorz, I. Komaromi, R. L. Martin, D. J. Fox, T. Keith, M. A. Al-Laham, C. Y. Peng, A. Nanayakkara, M. Challacombe, P. M. W. Gill, B. Johnson, W. Chen, M. W. Wong, C. Gonzalez, J. A. Pople, Gaussian, Inc., Wallingford CT, **2004**.
[43] The latter assignment is corroborated by comparison to a pyrrolidine-substituted Ru bis-terpyridine complex that features a similar LMCT band in the Ru^{III} state.[36]
[44] K. Nördstrom, E. Macedo, C. Moberg, *J. Org. Chem.* **1997**, *62*, 1604–1609.
[45] J. Wang, G. S. Hanan, *Synlett* **2005**, 1251–1254.
[46] E. Figgemeier, V. Aranyos, E. C. Constable, R. W. Handel, C. E. Housecroft, C. Risinger, A. Hagfeldt, E. Mukhtar, *Inorg. Chem. Commun.* **2004**, *7*, 117–121.
[47] E. C. Constable, A. M. W. Cargill Thompson, D. A. Tocher, M. A. M. Daniels, *New J. Chem.* **1992**, *16*, 855–867.
[48] O. Johansson, *Synthesis* **2006**, 2585–2589.
[49] M. Rudolph, *J. Comput. Chem.* **2005**, *26*, 633–641.
[50] M. Rudolph, *J. Electroanal. Chem.* **2004**, *571*, 289–307.

Received: June 19, 2008
Revised: September 30, 2008
Published online: December 15, 2008

